EMI-Induced Failures in Crystal Oscillators

Jean-Jacques Laurin, *Student Member, IEEE,* Safwat G. Zaky, *Member, IEEE,* and Keith G. Balmain, *Fellow, IEEE*

Abstract—**An EMI-induced failure mode pertaining to crystal-based voltage-controlled oscillators (VCO's) has been studied. The failure consists of a transition to a frequency of oscillation that differs from the crystal's fundamental resonant frequency, when the circuit is temporarily exposed to continuous or pulsed radio-frequency electromagnetic fields. The new state persists even after the EMI source is removed and leads to hang-up in digital systems. This mode transition has been observed experimentally. Its essential properties have been predicted theoretically and simulated numerically, using simplified oscillator models. The likelihood of observing such a failure in a noisy electromagnetic environment is assessed with respect to the radiated susceptibility levels given in MIL-STD-461B.**

I. Introduction

DURING radiated susceptibility tests such as those described in electromagnetic compatibility measurement standards [1] and tests on microcomputer boards [2], the equipment under test is exposed in its entirety to an incident electromagnetic field. In the case where the equipment fails to comply with its specified susceptibility limit, this method gives little insight into the nature of the failure mode. It is also difficult to identify any particular component that may be sensitive to external fields.

It was conjectured by the authors that a susceptibility mapping experiment might alleviate this difficulty, and such a technique was applied to an MC6809-based microcomputer board. The activity of the board is monitored by an interference-free computer which also controls the experiment. A 25-mm diameter loop antenna is positioned at a fixed height of about 5 mm above the plane of the board. The plane of the loop can be either parallel or perpendicular to the plane of the board. Because of the small size of the antenna and its close proximity to the board, it generates fields that are mostly concentrated over a small area of the board. A radio frequency current of controlled frequency and amplitude is fed to the antenna. The RF current is increased until a failure occurs in the board's operation. This test is repeated over an X–Y array of loop positions that spans the entire board. The triplets (X, Y, loop current at failure) are used to create a susceptibility map which helps to identify the circuit components that are the most affected by interference.

Susceptibility mapping led to the identification of the voltage-controlled oscillator (VCO) as a device that is sensitive to radio frequency interference (RFI). Frequencies in the range 20 to 100 MHz were used. When the antenna was placed in the vicinity of the VCO, failure occurred at RF current amplitudes that were considerably lower than for other locations on the board. Furthermore, in some cases, correct operation could not be restored until power to the 6809 board was turned off and then on again. It was not sufficient to activate the reset line on the board. Closer examination revealed that the interfering RF signal caused the 22-MHz oscillator to switch to a frequency of about 50 MHz, which persisted after the interfering signal was removed.

Oscillators similar to the type on the 6809 board are widely used to generate clock signals in digital systems. In this paper, the failure mode that leads to a permanent transition of the oscillator's frequency of operation is investigated. Experimental conditions in which oscillator interruptions have been observed are reported. An interpretation of the observed phenomena based on the theory of nonlinear circuits is given along with an example of numerical simulation showing an RFI-induced transition of oscillation frequency.

II. Experimental Observations

The high susceptibility of oscillators to RFI was observed during a mapping experiment on an MC6809-based microcomputer board. When a small loop antenna producing RFI fields was located in the neighborhood of the VCO chip, three types of failure were observed: 1) the microcomputer operations were perturbed to a point where computational errors occurred; 2) communication with the microcomputer via its serial port was disrupted by changes in the baud rate; 3) application of a short burst of RFI led to a permanent interruption of the clock signal on the board.

The first two failure modes were observed at many loop positions over the board. However, the third mode occurred only when the loop was in the vicinity of the traces connecting the VCO to the crystal, suggesting that failure in the analog section of the VCO was the likely cause for the interruption of the clock. This conjecture was tested by using a spectrum analyzer to monitor emission levels over the board. During normal operation, emissions at the clock's fundamental frequency (22.1 MHz) and its harmonics (44.2, 66.3 MHz, etc.) were recorded over many areas of the board. After applying a short burst of RFI, these spectral components vanished and high-frequency ($\approx$ 50 MHz) emissions were observed near the oscillator. The latter emissions are clearly attributable to an abnormal mode of oscillation of the VCO. The frequency of these oscillations seems to be too

Manuscript received August 30, 1990; revised March 1, 1991. This work was supported primarily by Bell Canada, and also by the Ontario University Research Incentive Fund, the Natural Sciences and Engineering Research Council of Canada, and the Information Technology Research Centre of Ontario.

The authors are with the Department of Electrical Engineering, University of Toronto, Toronto, Ont., Canada, M5S 1A4.

IEEE Log Number 9102198.

high to be amplified by the buffer at the output stage of the VCO, as evidenced by the absence of the clock signal at the output of the VCO.

Two types of VCO chips were tested, Texas Instruments 74LS629 and 74S124, with a 22.1184 MHz quartz crystal. In order to study their susceptibility separately from the other elements on the microprocessor board, each was mounted above a ground plane with crystal leads coupled to the disturbing loop as shown in Fig. 1. The leads connecting the crystal package to the VCO chip had a diameter of 1.3 mm and formed a loop of 25 mm diameter. The disturbing current was fed to a loop of identical diameter made of 2.25 mm diameter wire, placed coaxial with the crystal loop and at a distance of 5 mm. The two loops were placed above a ground plane, with their common axis parallel to the plane and 25 mm away from it. Measurement of the impedance matrix of the two-port network defined by the input terminals of two loops having a similar geometry and the same location above the ground plane revealed that for frequencies under 100 MHz, the self-impedance of each loop could be modeled by a 44-nH inductor and that the coupling between the two is mostly magnetic with a mutual inductance of 15 nH. It should be mentioned that the lead length used for the crystal is longer than that recommended for normal operation. It was used here to ensure that coupling to the crystal port of the VCO predominated over coupling to other ports. As a result, the failure modes pertaining to the section of the oscillator circuit connected to the crystal port should be more easily observable. The control inputs of the VCO, which are used to adjust the oscillation frequency, were set to the levels recommended by the manufacturer to give stable operation near 22 MHz (RNG = 0 volts and FC = 5 V [3]).

In the first step of the experiment, RF current of fixed amplitude and frequency was fed for about 2 s into the disturbing loop. Then, the same loop was connected to a spectrum analyzer for monitoring emissions from the device under test. Fig. 2 shows examples of emission spectra before and after the RF pulse was applied. Before applying the RFI pulse, harmonics of the crystal's fundamental frequency dominate. After applying the interference, the emission peaks are shifted to harmonics of 53 MHz, indicating a transition to a different mode of oscillation. When a small capacitor (a few pF) is connected in parallel with the crystal, the frequency of this new mode decreases, indicating the possible dependence of the mode on the parasitic capacitance associated with the crystal package and the pins of the VCO chip.

A transition from the 22.1-MHz mode to the higher frequency mode occurs easily when the disturbing signal frequency is between 30 and 70 MHz. The minimum amplitude of the current in the disturbing loop to induce the transition may be as low as 20 mA rms. According to the loop self and mutual inductances given above, the corresponding EMF around the VCO-crystal circuit loop induced by a 50-MHz RFI current fed to the disturbing loop antenna would be 91.2 mV rms. Digital devices usually found on microcomputer boards have noise margins that are decidedly larger than that (TTL: 0.6 V for low state and 0.4 V for high state [4], CMOS: 1.45 V in both states [5]). Therefore, it is easy to understand why the susceptibility mapping experiment identified the crystal oscillator as one of the most sensitive devices on the microcomputer board that was tested.

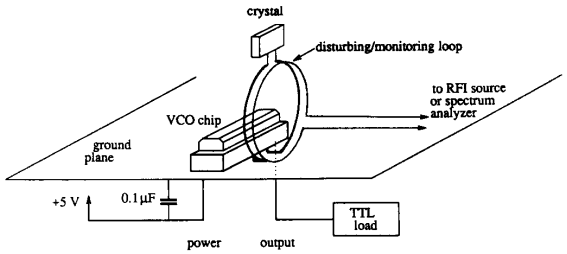

Fig. 1. Experimental set-up for VCO testing.

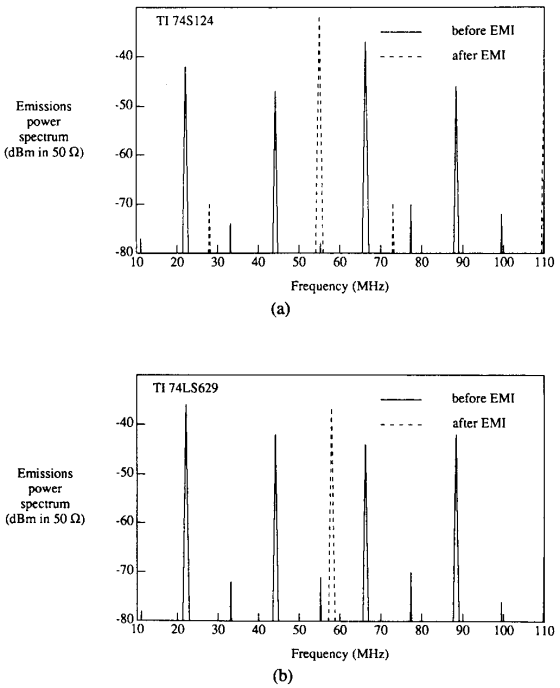

Fig. 2. Emissions in the vicinity of the VCO before and after an interfering signal is applied, for two types of VCO chips.

III. Circuit Model

Voltage-controlled oscillators used to derive clock signals in digital systems are usually composed of two functional subsystems. The first part is an analog positive feedback amplifier, loaded with a tuned circuit selected to obtain the desired frequency of operation. If the tuning device is a capacitor, the dc bias of the control inputs must be carefully adjusted in order to obtain the desired frequency. The control inputs are used to change the quiescent point of the transistors from which the positive feedback amplifier is built. Depending on the quiescent point, the gain and the bandwidth of the amplifier are modified, which results in a modification of the oscillation frequency. There are two control inputs on the Texas Instruments 74S124 and 74LS629 chips used in

this paper. Instead of a capacitor, a high-Q resonant circuit such as a quartz crystal can be used as a tuning device. In this case, the frequency of operation is fixed and the adjustment of the control inputs is not so crucial. The commonly available 0 and +5 V levels could then be connected to the controls in a manner that will guarantee stable oscillations at the crystal's fundamental resonant frequency. The oscillator's output is fed to a buffer stage that converts the oscillatory analog signal to the appropriate voltage and impedance levels for a transistor-transistor-logic (TTL) environment. In what follows, the buffer stage is of no interest and will be omitted in the VCO models used.

A simplified model of the analog section of the VCO is depicted in Fig. 3. The lumped elements L_1, C_1, and R_1 determine one of the resonances of the quartz crystal. The analog port of the VCO chip, labeled CX on VCO data sheets, is modeled by a nonlinear resistor R^- that obeys the voltage–current relationship

$$v = -ai + bi^3. \tag{1}$$

The inductance of the leads connecting the crystal to the CX port is represented by L_c. In configurations where the VCO and crystal are not packaged together in a metal enclosure, the crystal leads can provide magnetic coupling to external RFI fields which induce voltages in the analog port-crystal loop. External interference is modeled by an RFI current source I_s and the inductor L_c' coupled to L_c.

Let us assume now that parasitic elements can be represented by a series resonator (L_2, C_2, R_2) connected in parallel with the nonlinear resistor. The resulting circuit, depicted in Fig. 4, forms a two-resonator oscillator. Its dual version (two parallel resonators in series) has been studied by Bertrand *et al.* [6] for nonlinearities involving terms of powers 2 and 3, and by Bruyland [7] for nonlinearities involving terms of powers 3 and 5. More recently, Sommariva [8] generalized the analysis to oscillators having an arbitrary number of resonators. Experimental work on such topologies has been presented by Edson [9] based on the theoretical work of van der Pol [10]. All these authors agree on the fact that under certain conditions, the circuit of Fig. 4 can give rise to two modes of oscillation, each at a frequency that is in the neighborhood of the resonance frequencies of the LCR branches. They also found that a mode involving a superposition of these two basic frequency components is not stable if the nonlinearity is only cubic.

Predicting the possible modes of operation of an oscillator with linear theory, as was done by Unkrich and Meyer [11], and Gibbons [12], leads to the existence conditions for each mode, but does not provide information on mode stability. Following a method presented by Hale [13], the circuit in Fig. 4 has been analyzed in order to derive the existence and stability conditions for periodic solutions. The main steps of the analysis can be found in the Appendix. The analysis revealed that three stable modes of operation exist. To a first level of approximation, the solution in each of these modes has the form:

$$i_1(t) = i_{10} \sin(\omega_1 t + \phi_1) \qquad i_2(t) = i_{20} \sin(\omega_2 t + \phi_2)$$

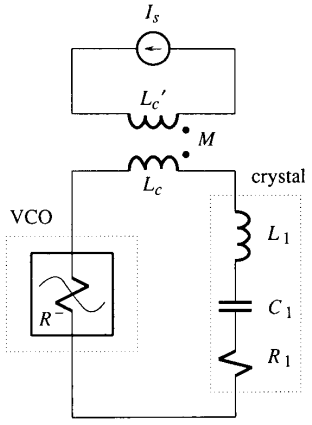

Fig. 3. VCO-crystal model with coupling to interference source.

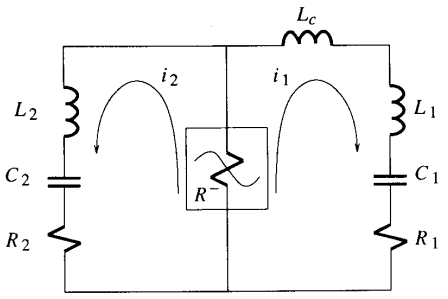

Fig. 4. Two-mode oscillator model for the VCO.

where $\omega_1^2 = 1/(L_1 + L_c)C_1$ and $\omega_2^2 = 1/L_2C_2$, provided that ω_1/ω_2 is not a rational number. The constants ϕ_1 and ϕ_2 depend on the initial conditions. The constants i_{10} and i_{20} are given by

mode 1:

$$i_{10} = \sqrt{\frac{4(a - R_1)}{3b}}, \qquad i_{20} = 0 \tag{2}$$

mode 2:

$$i_{10} = 0, \qquad i_{20} = \sqrt{\frac{4(a - R_2)}{3b}} \tag{3}$$

mode 3:

$$i_{10} = i_{20} = 0.$$

Fig. 5 summarizes the existence and stability conditions for these three modes as functions of a, R_1, and R_2. Parameter b does not affect the stability; however, it is assumed to be finite and positive. Depending on the values of R_1/a and R_2/a, a mode exists (E), is stable (S), or does not exist (no symbol), as indicated in various areas of the graph.

The circuit considered above is a highly simplified model of a crystal oscillator circuit. In a more realistic model, the origin of the components giving rise to the higher-frequency mode, represented by a parasitic RLC branch in Fig. 4,

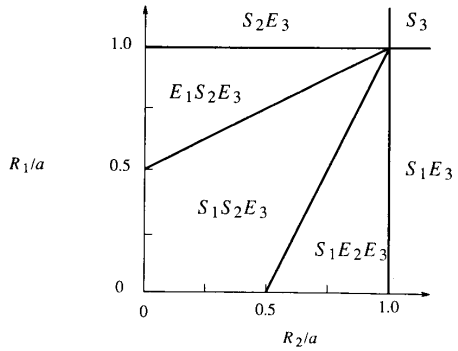

Fig. 5. Existence (E) and stability (S) regions of modes 1, 2 and 3 as a function of R_1, R_2, and a for the circuit of Fig. 4. (e.g., $E_1S_2E_3$ means that mode 2 is stable while modes 1 and 3 exist but are not stable.)

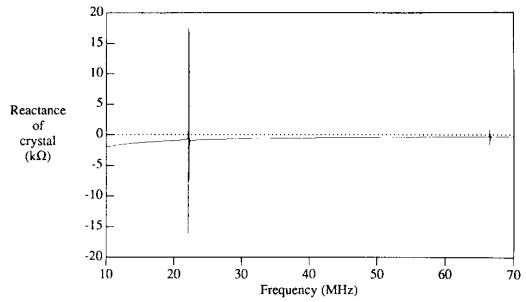

Fig. 6. Measured reactance of the crystal unit. The operation frequency specified by the manufacturer is 22.1184 MHz.

would have to be specified. For the oscillators used in the experiments, it might be possible that this parasitic resonator is associated with an overtone of the crystal. In such a case, the input impedance of the crystal would have a resonance at a frequency that is close to the frequency components detected after the application of interference (see Fig. 2). Fig. 6 shows a plot of the measured reactance of the crystal unit versus frequency. The main features are observable near 22.1 MHz, which corresponds to the crystal's fundamental mode, and also near the harmonic overtone 66.3 MHz. Higher frequency resolution sweeps revealed the presence of several anharmonic overtone resonances in the vicinity of 22.1 MHz and 66.3 MHz but not in the frequency range corresponding to the observed higher frequency mode of oscillation. The crystal behaves like a capacitor of about 10 pF, except near the odd harmonics of 22.1 MHz.

In another experiment, small capacitors were connected in place of the crystal unit. The oscillation frequency of the higher frequency mode is given for three cases in Table I. Without the presence of the crystal, oscillation takes place in the 48–55 MHz range and the 22.1 MHz mode does not exist. The chip + crystal case has a frequency that is between the frequencies of the chip + 10 pF and chip + 5 pF cases. This suggests that, as far as the parasitic mode is concerned, the crystal behaves like a capacitor having a value somewhere between 5 pF and 10 pF. Assuming a value of 10 pF, the capacitor, if connected in series with the 44-nH inductance of the leads, would form a 240-MHz series resonator. Since this frequency is well above the observed frequency of the parasitic mode, it is clear that the reactive nature of the VCO chip's crystal port must be taken into account. This is not unexpected because, as mentioned earlier, the data sheets of the VCO chips specify that these units can be operated with a capacitor as a tuning device. When a crystal is used as a tuning device, the VCO chip can operate in two different modes: a "crystal mode" and a "capacitor mode."

Fig. 7 gives an improved model for the crystal and the analog section of the VCO. The crystal is represented by a series resonator shunted with a capacitor C_c associated with the package, as shown in Fig. 7(a). For Texas Instruments 74LS629 VCO's, the crystal is connected between the two

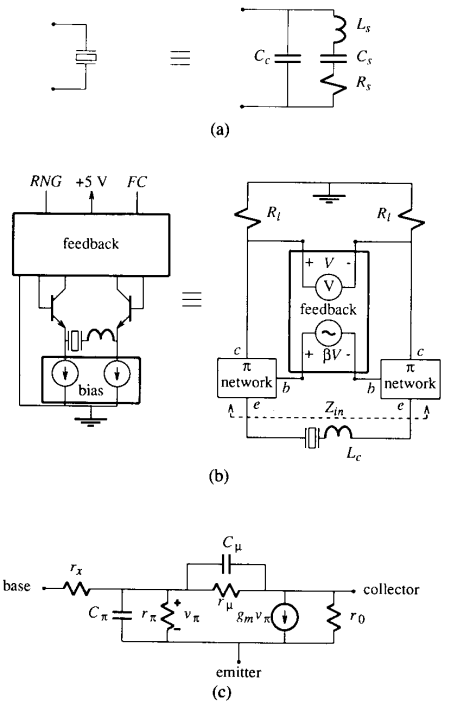

Fig. 7. VCO and crystal models: (a) crystal including package capacitance C_c; (b) differential amplifier with feedback and its equivalent idealized small-signal model; (c) the small-signal network model for the bipolar transistors. L_c in part (b) represents the inductance of the crystal leads.

TABLE I
OSCILLATION FREQUENCY OF THE HIGHER FREQUENCY MODE FOR DIFFERENT LOADS ON THE VCO CHIP

Circuit configuration	Frequency of higher-frequency mode (MHz)
Chip + 10 pF	48.8
Chip + crystal	52.6
Chip + 5 pF	54.0

emitters of a differential amplifier. An active feedback network samples the voltage between the two collectors and applies a proportional signal between the bases of the differential pair (shunt-series feedback). This circuit and its model are depicted in Fig. 7(b). The feedback network is repre-

sented by a voltage-controlled voltage source having a voltage gain β (= output voltage/controlling voltage). The two resistors R_l represent the collector loads, which in the 74LS629 consist of transistor networks to which the control inputs are connected to adjust the gain of the amplifier.

Over a limited frequency range, the circuit of Fig. 7(b) can be replaced with the simplified model shown in Fig. 8. To account for the nonlinearity of the transistor pair, a saturating cubic term is added to the current voltage characteristic of the box labeled R^-, as in (1). The parameters of the model in Fig. 8 are chosen as follows. First, the transistors of the differential pair are replaced with their π model shown in Fig. 7(c), using parameters that are typical of IC NPN transistors. The impedance Z_{in} between the two transistor emitters is calculated. Then, the values of a (the coefficient of the linear term of R^-), R_{pole} and L_{pole} are chosen to make the impedance Z_{in} in Fig. 8 as close as possible to the impedance seen in the crystal in the small-signal model of Fig. 7(b). The real and imaginary parts of Z_{in} of the two circuits for the selected parameters are plotted versus frequency in Fig. 9. It should be noted that the agreement between the two impedances is good over the frequency range that can give rise to oscillation (Re $\{Z_{in}\} < 0$).

Unfortunately, the resulting nonlinear oscillator model in Fig. 8 is difficult to analyze. This is because the differential equations of the system cannot be cast in a form that makes possible the use of the techniques proposed in [8] or [13]. A heuristic approach based on the stability analysis of linear systems is proposed instead. First, the impedance versus frequency seen by the nonlinear resistor R^- is calculated. The frequencies for which the impedance is purely resistive and is smaller than parameter a are the potential frequencies of oscillation of the system. In the case where only two frequencies ω_1 and ω_2 exist, the circuit can be assumed to behave like that of Fig. 4 near the oscillation frequencies. Resistances R_1 and R_2 are the real part of the impedance seen by R^- at ω_1 and ω_2. These resistances, together with the parameter a, can be used in conjunction with Fig. 5 to evaluate the stability of the oscillatory solutions. Equations (2) and (3) can then be used to obtain an approximate amplitude for the current in each mode.

Fig. 10 shows a plot of the imaginary part of the impedance seen by R^- versus frequency. The existence of the higher frequency mode can be understood by comparing this curve to the measurement of the crystal's reactance (Fig. 6) in which the effect of L_{pole} and R_{pole} is not included. The positive reactance of the parallel combination of L_{pole} and R_{pole}, when added to the negative reactance of the crystal's capacitance, causes the total reactance to be zero near 55 MHz as in Fig. 10. This zero crossing is responsible for the existence of the higher frequency mode.

Fig. 11, obtained by SPICE simulations of the oscillator model (see Fig. 8), illustrates how a disturbance produced by the external source I_s can induce self-sustained oscillations at a different frequency in $i_{R^-}(t)$. For this simulation, the inductance L_c is coupled to another inductance L_c' as in Fig. 3. Inductance L_c' is fed with the pulsed RF current source I_s. Note that according to Fig. 5 the values of a (939 Ω), R_1

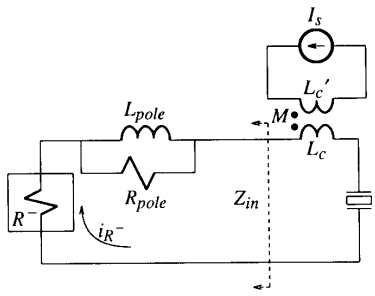

Fig. 8. Simplified model derived from Fig. 7. In the simulations, $L_c = L_c'$ = 44 nH, M = 15 nH, L_{pole} = 1.45 μH, R_{pole} = 1194 Ω; for R^- as defined in (1), a = 939 Ω and $b = 3 \times 10^8$ VA^{-3}; for the crystal defined in Fig. 7(a), C_c = 6.5 pF, L_s = 520 μH, C_s = 0.1 pF, and R_s = 30 Ω.

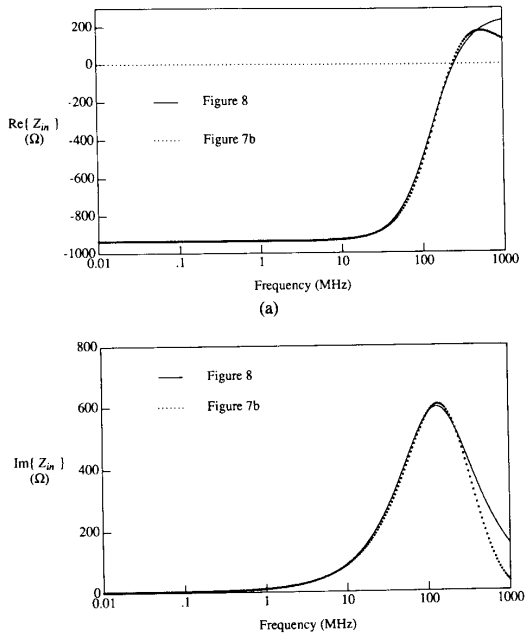

Fig. 9. Impedance seen by the crystal in the circuits of Fig. 7(b) and the linearized version of Fig. 8. The parameters used are a = 939 Ω, L_{pole} = 1.45 μH, R_{pole} = 1194 Ω in Fig. 8 and R_l = 500 Ω, $\beta = -1$, r_x = 2500 Ω, r_ω = 50 MΩ, r_0 = 0.1 MΩ, g_m = 40 mA/V, C_π = 10 pF and C_μ = 1 pF in Fig. 7.

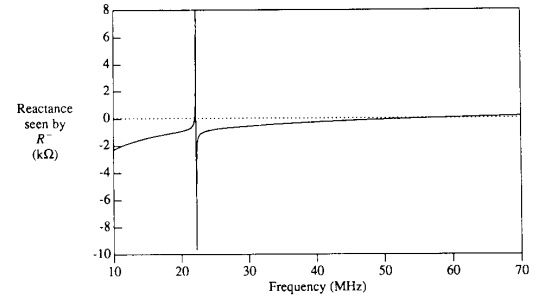

Fig. 10. Reactance seen by R^- in the circuit of Fig. 8 when the current source I_s is replaced with an open circuit.

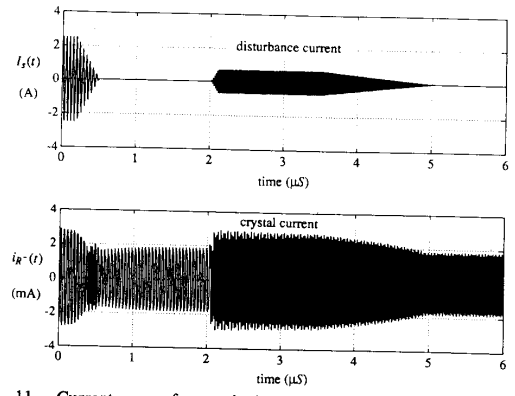

Fig. 11. Current wave forms obtained from SPICE simulation for the circuit of Fig. 8.

TABLE II
AMPLITUDES AND FREQUENCIES OF A TWO-MODE OSCILLATOR PREDICTED WITH ZERO ORDER APPROXIMATION AND OBTAINED WITH SPICE SIMULATIONS

	VCO current, i_{R^-}	Amplitude (mA peak)	Frequency (MHz)
MODE 1	Analysis	1.98	22.0
	Simulation	2.16	21.9
	Experiment 74S124	1.21	22.1
	Experiment 74LS629	2.43	22.1
MODE 2	Analysis	1.84	55.4
	Simulation	1.99	48.8
	Experiment 74S124	1.60	55
	Experiment 74LS629	0.86	58

(52.9 Ω), and R_2 (181.1 Ω) allow stability for modes 1 and 2. The external source I_s first excites mode 1 with a short burst of 22.1 MHz signal, after which the oscillator rapidly stabilizes to a frequency of about 22 MHz. Then, a burst of 55.3 MHz signal is applied by I_s to induce a transition to $\approx$ 55 MHz oscillations (mode 2). Table II shows how the simulation results compare to those obtained from the heuristic method described previously. The magnitude and frequency of the simulated waveform were obtained after the system had reached steady-state in each mode. Also shown are the crystal loop current magnitudes and frequencies obtained experimentally for one specimen of each chip (74S124 and 74LS629). These numbers were calculated with the emission spectrum data (Fig. 2) and by taking into account the mutual and self-inductances of the loops as well as the spectrum analyzer's input impedance (50 Ω).

In spite of the fact that the heuristic approach was based on the analysis of a circuit (Fig. 4) having a different topology from the circuit simulated (Fig. 8), the agreement between the quantities predicted and the results of the numerical simulation is good. Thus, it seems that when R^- is connected to a circuit having two series resonances, the modes of oscillation are similar in frequency and amplitude to the modes obtained when R^- is actually connected to two series-LCR branches in parallel. Of course, there is no guarantee that this result would hold in general. Also, it should be recalled that the formulas used for amplitude and frequency predictions were derived from a zero-order analysis and should become less precise for strong nonlinearities, that is, for large values of b in (1). In the example presented here, the oscillation frequencies ω_1 and ω_2 at which the impedance seen by R^- is purely resistive barely change when the inductances L_c and L_c' modeling the crystal leads and the disturbing loop are not taken into account in the impedance calculation. Nevertheless, the mutual inductance between these loops is essential to achieve coupling with the RFI source.

Using a simplified model for the VCO-crystal circuit, it has been shown that self-sustained oscillations at two different frequencies can be stable. Fig. 11 further indicates that it is possible to induce switching to another mode of oscillation by applying a short burst of RFI coupled from an external source.

IV. DISCUSSION

The mode switching phenomenon described in the previous section can lead to failures in digital systems. However, the probability of inducing such failures should be estimated for the electromagnetic environment in which digital systems operate. For the configuration depicted in Fig. 1, mode switching was achieved at a fairly low RFI current level, because of the good magnetic coupling between the VCO loop and the source of disturbance. This is not always the case in practical situations where electromagnetic field sources may be far away. Also, the wire loop formed by the leads connecting the VCO chip to the crystal are usually kept short in order to reduce emissions and pickup of electromagnetic fields.

As an example of external EMI, consider the case of a uniform electromagnetic plane wave incident on a VCO-crystal loop forming a 1 cm × 1 cm square. For a thin wire loop that is small relative to the wavelength of the incident wave, the induced current can be assumed constant around the loop. In this case, it can be shown that

$$\text{effective length} \approx 2L \sin(\pi L/\lambda)$$

where L is the length of each of the square sides. At 50 MHz, the effective length for L = 1 cm is about 1.05×10^{-4} m. At this frequency, it was mentioned in Section II that an induced voltage of about 100 mV rms is needed to trigger mode switching in the oscillator. This requires an incident wave amplitude of 1347 V/m peak, which is well above U.S. military standards for radiated susceptibility. These standards stipulate that electronic equipment should be able to withstand fields of 200 V/m peak [14], 10 V/m peak [15], or 5 V/m peak [16] depending on the class of equipment.

Larger structures in a digital system, such as power and ground lines, are, in general, more efficient antennas than the small loop mentioned previously. They could have larger induced currents for the same level of external electromagnetic field. If such lines are in the vicinity of the VCO-crystal loop, the scattered field they produce may be sufficient to

cause an oscillator failure. For example, assume that the VCO-crystal loop is near a half-wavelength wire as shown in Fig. 12, and that all the wires are 1 mm in diameter. For a 1-cm square loop with its center 1.0 cm away from the antenna, the effective length relating the incident electric field to the open-circuit voltage is approximately 1.5×10^{-2} m. This number has been obtained with a modified version of Richmond's method-of-moments program [17], [18], and is nearly constant for frequencies between 20 and 100 MHz. Fig. 13 gives the induced EMF in the loop as a function of frequency for incident fields of 200, 10, and 5 V/m peak. Also shown is the failure level obtained for a 74LS629 chip operated with a 22.1 MHz crystal. Clearly, the susceptibility threshold of the VCO is well below the requirement of the 200 V/m standard, at all frequencies tested.

The example above shows that even though the wire structures connecting a susceptible device, such as the VCO, can be made very small, the scattered field from neighboring wires can easily lead to a failure threshold for an incident field that is below existing standards. For a susceptibility threshold of 100 mV rms of induced EMF, effective lengths of only 0.7 mm and 28.2 mm, respectively, are required to cause failure at the 200 V/m and 5 V/m incident field levels specified by military standards. These very low figures emphasize the importance of considering RFI effects when designing the layout of a printed circuit board.

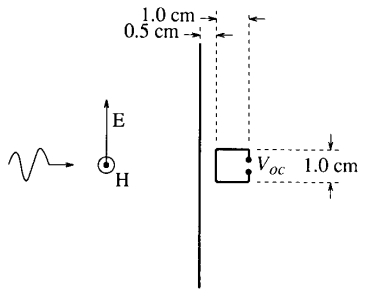

Fig. 12. A small square loop located near a half-wave dipole and illuminated by a uniform plane wave.

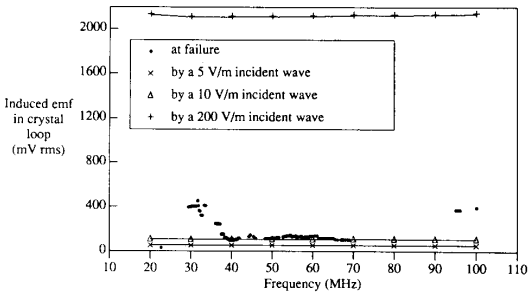

Fig. 13. Comparison between the voltage induced at the crystal port of a 74LS629 to cause mode switching and the open circuit voltage at the loop of Fig. 12 for incident plane waves of 200, 10, and 5 V/m peak.

V. Conclusions

In this paper, a failure mode pertaining to oscillators exposed to continuous-wave electromagnetic interference has been investigated. During susceptibility mapping experiments, it was observed that small amplitudes of interfering current at frequencies around 50 MHz induce switching to a second mode of oscillation in crystal-operated 74S124 and 74LS629 (Texas Instruments) VCO chips. Under certain conditions, the new state persisted after the removal of the interfering source. The change in the oscillator's frequency causes failure in the operation of the digital system connected to the oscillator.

A two-resonator circuit has been used to model the crystal oscillator. The conditions necessary for the existence and stability of two modes of oscillation for this model were obtained using nonlinear circuit analysis. It has been found that the model can also be used to predict the amplitude and frequency of oscillation with good precision. The results were verified using SPICE simulations.

The external field intensity needed to induce the RF voltage to cause mode switching in an oscillator loop of typical dimensions is quite high—of the order of 1400 V/m. However, it has been shown that scattering from nearby long conductors can reduce the failure threshold to a value at or not far above the 5 V/m and 10 V/m susceptibility standard and well below the 200 V/m susceptibility standard.

Appendix

Applying Kirchhoff's voltage law to the circuit of Fig. 4 generates the following equations:

$$L_j \frac{d^2 i_j}{dt^2} + R_j \frac{di_j}{dt} + \frac{i_j}{C_j} = \left[a - 3b(i_1 + i_2)^2\right]\left[\frac{di_1}{dt} + \frac{di_2}{dt}\right] \qquad j = 1, 2$$

in which L_c has been included in L_1.

The difficulty in investigating the existence and stability conditions of periodic solutions for this system comes from the fact that the oscillator has two degrees of freedom. In such a case, the conditions leading to dynamic equilibrium (stable oscillations) are difficult to obtain. Fortunately, existence and stability conditions for the aforementioned system can be derived from the theorems presented by Hale [13]. For certain classes of nonlinear systems, it is sown that an averaging process can be used to reduce the analysis of dynamic equilibrium (orbital stability) to the analysis of static equilibrium (nodal or local stability). This allows the application of well established techniques to assess local stability of nonlinear systems with more than one degree of freedom.

The following change of variables is first performed.

$$x_1 = i_1 \qquad x_3 = i_2 \qquad x_2 = \dot{x}_1 \qquad x_4 = \dot{x}_2$$

in which the dot stands for time derivative. This leads to the vector system of equations:

$$\dot{x} = Ax + f$$

where

$$A = \begin{bmatrix} 0 & 1 & 0 & 0 \\ -\omega_1^2 & 0 & 0 & 0 \\ 0 & 0 & 0 & 1 \\ 0 & 0 & -\omega_2^2 & 0 \end{bmatrix}, \quad f = \begin{bmatrix} 0 \\ f_1 \\ 0 \\ f_2 \end{bmatrix},$$

$$\omega_j^2 = 1/L_jC_j,$$

and

$$f_j = \frac{1}{L_j}\left[(a - 3b(x_1 + x_3)^2)(x_2 + x_4) - R_j x_{2j}\right].$$

Using a substitution due to van der Pol [10], namely

$$x_1 = \rho_1 \sin(\omega_1\gamma_1) \qquad x_2 = \rho_1\omega_1 \cos(\omega_1\gamma_1)$$

$$x_3 = \rho_2 \sin(\omega_2\gamma_2) \qquad x_4 = \rho_2\omega_2 \cos(\omega_2\gamma_2)$$

we obtain

$$\dot{\boldsymbol{\rho}} = \epsilon \boldsymbol{R}(\boldsymbol{\gamma}, \boldsymbol{\rho}) \qquad \dot{\boldsymbol{\gamma}} = \mathbf{1} - \epsilon \boldsymbol{\Gamma}(\boldsymbol{\gamma}, \boldsymbol{\rho}) \qquad \text{(A1)}$$

where

$$R_1 = f_1 \cos(\omega_1\gamma_1) L_1/(a\omega_1)$$

$$R_2 = f_2 \cos(\omega_2\gamma_2) L_1/(a\omega_2)$$

$$\Gamma_1 = f_1 \sin(\omega_1\gamma_1) L_1/(a\rho_1\omega_1^2)$$

$$\Gamma_2 = f_2 \sin(\omega_2\gamma_2) L_1/(a\rho_2\omega_2^2)$$

and $\epsilon = \dfrac{a}{L_1}$. Since (A1) is in the form of eq. 18-1 in [13], theorem 18-1 in [13] applies. Let $\boldsymbol{R}_0(\boldsymbol{\rho})$ be the average of $\boldsymbol{R}(\boldsymbol{\gamma}, \boldsymbol{\rho})$ over the τ space; that is

$$\boldsymbol{R}_0(\rho) = \lim_{T\to\infty} \frac{1}{T} \int_0^T \boldsymbol{R}(\boldsymbol{\gamma} + \tau, \boldsymbol{\rho})\, d\tau,$$

$$\boldsymbol{\gamma} + \tau = \begin{bmatrix} \gamma_1 + \tau \\ \gamma_2 + \tau \end{bmatrix}$$

According to theorem 18-1 in [13], the solution of A1 to a zeroth-order in ϵ is given by

$$\rho_1 = \rho_{10}, \qquad \rho_2 = \rho_{20}, \qquad \gamma_{10} = t + t_1, \qquad \gamma_{20} = t + t_2$$

where t_1 and t_2 are constants depending on initial conditions and ρ_{10}, ρ_{20} are the solutions of

$$\boldsymbol{R}_0(\boldsymbol{\rho}) = \mathbf{0}. \qquad \text{(A2)}$$

Evaluation of the above integrals allows us to rewrite the determining equation (A2) in the following form:

$$\rho_1\left[\rho_1^2 + 2\rho_2^2\right] - 4\rho_1\frac{a - R_1}{3b} = 0$$

$$\rho_2\left[2\rho_1^2 + \rho_2^2\right] - 4\rho_2\frac{a - R_2}{3b} = 0$$

for which four solutions can be found. These are

$$\rho_{10} = \sqrt{\frac{4(a - R_1)}{3b}}, \qquad \rho_{20} = 0$$

$$\rho_{10} = 0, \qquad \rho_{20} = \sqrt{\frac{4(a - R_2)}{3b}}$$

$$\rho_{10} = \rho_{20} = 0$$

$$\rho_{10} = \sqrt{\frac{4(a - 2R_2 + R_1)}{9b}},$$

$$\rho_{20} = \sqrt{\frac{4(a - 2R_1 + R_2)}{9b}}.$$

Existence of these solutions requires the expressions under square roots to be positive. The stability condition for each of these four solutions is the same as for local stability near the solution $\boldsymbol{\rho} = \mathbf{0}$ of the linear system:

$$\dot{\boldsymbol{\rho}} = \boldsymbol{J}\left[\boldsymbol{R}_0(\boldsymbol{\rho})\right]\big|_{\rho=\rho_0}\boldsymbol{\rho}$$

where $\boldsymbol{J}$ is the Jacobian matrix calculated with respect to the independent variables ρ_1 and ρ_2 and evaluated at $\boldsymbol{\rho} = \boldsymbol{\rho}_0$. A solution will be stable if the eigenvalues of $\boldsymbol{J}$ have a negative real part. By performing the appropriate arithmetic, it can be shown that the parameter b does not affect the existence and stability conditions if b is assumed to be positive. Fig. 5 depicts the regions of the $R_1/a - R_2/a$ plane where these conditions are satisfied for the first three solutions of (A2). The fourth solution does not appear in the figure because its regions of existence and stability do not overlap. This is in agreement with Bruyland [7] who found that a solution involving a superposition of two different basic frequencies is not possible when the nonlinearity is cubic.

Substituting $\boldsymbol{\rho}_0$ and $\boldsymbol{\gamma}_0$ into the 4-element vector $\boldsymbol{x}$, and calculating $\boldsymbol{i}$ from x_1 and x_3 leads to the equations given in Section III for i_1 and i_2, namely

$$i_1(t) = i_{10} \sin(\omega_1 t + \phi_1) \qquad i_2(t) = i_{20} \sin(\omega_2 t + \phi_2)$$

Acknowledgment

The authors express their appreciation for the strong support and interaction provided by Bell Canada and Bell-Northern Research, and in particular by Mr. M. M. Cohen. The authors are grateful to Mr. G. R. Dubois for his technical assistance.

References

[1] *Measurement of Electromagnetic Interference Characteristics*, MIL-STD-462 (Notice 3), Feb. 1971, pp. 116–122.

[2] W. W. Everett, III and W. W. Everett, Jr., "Microprocessor susceptibility to RF signals—Experimental results," in *Proc. IEEE Southeastern Conf.*, 1984, pp. 512–516.

[3] *The TTL Data Book*, 2nd ed., Texas Instruments Inc., Dallas, TX, 1976, pp. 7-123–7-128.

[4] *The TTL Data Book, Vol. 2*, Texas Instruments Inc., Dallas, TX, 1985, p. 3-30.

[5] *CMOS Integrated Circuits Databook*, RCA Corp., Somerville, NJ, 1983, p. 58.

[6] G. Bertrand, A. Bonnot, and A. Lagouge Capiomont, "Simultaneous oscillations in marginal oscillators," *IEEE Trans. Circuit Theory*, vol. CT-19, pp. 271–277, May 1972.

[7] I. Bruyland, "Simultaneous oscillations at two frequencies in RLC circuits," *Proc. IEEE*, vol. 56, pp. 82–83, Jan. 1968.

[8] A. M. Sommariva, "On the analysis of internally resonant oscillators," *IEEE Trans. Circuits Syst.*, vol. 35, pp. 221–229, Feb. 1988.

[9] W. A. Edson, "Frequency memory in multimode oscillators," *IRE Trans. Circuit Theory*, vol. CT-2, pp. 58–66, Mar. 1955.

[10] B. van der Pol, "The nonlinear theory of electric oscillations," *Proc. IRE*, vol. 22, pp. 1051-1086, Sept. 1934.
[11] M. A. Unkrich and R. G. Meyer, "Conditions for start-up in crystal oscillators," *IEEE J. Solid-State Circuits.*, vol. SC-17, pp. 87-90, Feb. 1982.
[12] J. F. Gibbons, "An analysis of the modes of operation of a simple transistor oscillator," *Proc. IRE,*, vol. 49, pp. 1383-1390, Sept. 1961.
[13] J. K. Hale, *Oscillations in Nonlinear Systems*. New York: McGraw-Hill, 1963, pp. 161-169.
[14] *Electromagnetic Emission and Susceptibility Requirements for the Control of Electromagnetic Interference*, MIL-STD-416B, Apr. 1980, Part 5.
[15] *Electromagnetic Emission and Susceptibility Requirements for the Control of Electromagnetic Interference*, MIL-STD-416B, Apr. 1980, Parts 2, 3, 4 and 9.
[16] *Electromagnetic Emission and Susceptibility Requirements for the Control of Electromagnetic Interference*, MIL-STD-416B, Apr. 1980, Parts 2, 3, and 4.
[17] M. A. Tilston and K. G. Balmain, "On the suppression of asymmetric artifacts arising in an implementation of the thin-wire method of moments," *IEEE Trans. Antennas Propagat.*, vol. 38, pp. 281-285, Feb. 1990.
[18] M. A. Tilston and K. G. Balmain, "A multiradius, reciprocal implementation of the thin-wire moment method," *IEEE Trans. Antennas Propagat.*, vol. 38, pp. 1636-1644, Oct. 1990.

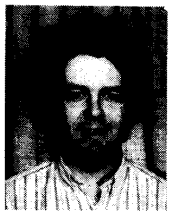

Jean-Jacques Laurin (S'87) was born in Le Gardeur, P.Q., Canada, in 1959. He received the B.Eng. degree in engineering physics from Ecole Polytechnique de Montréal, Montreal, P.Q., Canada, in 1983 and the M.A.Sc. degree in electrical engineering from the University of Toronto, Toronto, Ont., Canada, in 1986. He is currently working towards the Ph.D. degree in electrical engineering at University of Toronto. His research topic is the effect of electromagnetic interference on digital circuits.

Safwat G. Zaky (S'68-M'69) received the B.Sc. degree in electrical engineering and B.Sc. degree in mathematics, both from Cairo University, Cairo, Egypt, and the M.A.Sc. and Ph.D. degrees in electrical engineering from the University of Toronto, Toronto, Ont., Canada.

He is a Professor in the Departments of Electrical Engineering and Computer Science, University of Toronto. Prior to joining the University of Toronto, he was with Bell Northern Research, Bramalea, Ont., Canada, where he worked on applications of electrooptics and magnetics in mass storage and telephone switching. He was a Senior Visitor with the Computer Laboratory, University of Cambridge, England in 1980-1981. His current research interests are in the areas of computer architecture, logic synthesis, and electromagnetic compatibility of digital systems. He has coauthored two books on computer organization and microprocessor structures.

Dr. Zaky is a member of the Association of Professional Engineers of Ontario.

Keith G. Balmain (S'56-M'63-SM'85-F'87) was born in London, Ont., Canada, on August 7, 1933. He received the B.A.Sc. degree in engineering physics from the University of Toronto, Toronto, Ont., Canada, in 1957, and the M.S. and Ph.D. degrees in electrical engineering from the University of Illinois, Urbana, in 1959 and 1963, respectively.

He was an Assistant Professor of Electrical Engineering at the University of Illinois, Urbana, associated primarily with the Aeronomy Laboratory, until 1966. Then he joined the Department of Electrical Engineering at the University of Toronto where he is now a Professor and holder of the Bell Canada/NSERC Industrial Research Chair in Electromagnetics. He was Chairman of the Division of Engineering Science for two and one-half years until 1987, after which he was Chairman of the University of Toronto's Research Board for a three-year term. His research has focused on antennas in plasma, broadband antennas, radio wave scattering from power lines and high-rise buildings, electrostatic charge accumulation and arc discharges on synchronous-orbit spacecraft, and electromagnetic compatibility.

Dr. Balmain was corecipient of the IEEE Antennas and Propagation Society Best Paper of the Year award in 1970. He coauthored the second edition of *Electromagnetic Waves and Radiating Systems*. His activities include: Member of the IEEE Antenna Standards Committee and Chairman of the Subcommittee on Antennas in Physical Media (1968-1976); Canadian Chairman of the International Union of Radio Science Commission VI (1970-1973); member, IEEE APS AdCom (1973-1976); Associate Editor, *Radio Science* (1978-1980); Chairman, Technical Program Committee, 1980 IEEE APS International Symposium.